MTLA 42 (2025) 102453

Contents lists available at ScienceDirect

Materialia

journal homepage: www.elsevier.com/locate/mtla

Full Length Article

Planar coincident site density is not a reliable predictor of grain boundary energy

Eileen L. Hung, Zipeng Xu, Gregory S. Rohrer *

Department of Materials Science and Engineering, Carnegie Mellon University, Pittsburgh, PA 15213, USA

ARTICLE INFO

Keywords:
Grain boundary energy
Coincident site lattice
Planar coincident site density

ABSTRACT

The energies of grain boundaries in Ni and α-Fe have been compared to the planar coincident site density (PCSD) of grain boundaries with $\Sigma \leq 33$ in the FCC and BCC structures. The PCSD is not correlated to the energies and is therefore not a useful predictor of the grain boundary energy. Because grain boundary relative area is often an indicator of grain boundary energy, measured grain boundary areas are also compared to the PCSD and again no correlation is observed. The absence of a correlation likely arises from the fact that coincident sites at grain boundaries do not generally have local coordination environments that are similar to the bulk sites and are therefore not expected to lead to reduced grain boundary energies.

The planar coincident site density (PCSD) of a grain boundary is the number of coincident sites per grain boundary area [1,2]. The PCSD was hypothesized to be inversely correlated to grain boundary energy based on the idea that atoms situated at coincident lattice sites would in some way be more ideal than those at non-coincident sites. Sutton and Balluffi's [3] 1987 paper on geometric criteria for low energy interfaces critically examined the relationship between PCSD and grain boundary energy and concluded that the existing data provided no support for the hypothesis that they were related.

We were motivated to re-examine this hypothesis for three reasons. First, earlier formulae to compute the PCSD contained an error that has recently been corrected by Morawiec [4], and this makes an improved comparison possible. The second reason is that the data available for comparison in 1987 was relatively sparse. Since that time, the expanded capabilities of atomistic computer simulations to compute grain boundary energies [5], the ability to measure relative grain boundary energies from three-dimensional microstructure data [6,7], and the ability to measure grain boundary relative area distributions [8] has led to a comparative wealth of data that can be used to test the PCSD hypothesis. Third, despite Sutton and Balluffi's [3] conclusion that there is no support for the hypothesis that planar coincident site density is a predictor of grain boundary energy, it is not unusual to read contrary assertions in the contemporary materials science literature, particularly with reference to "special" boundaries.

As a test of the hypothesis, we will use the planar coincident site densities computed using Morawiec's [4] formula for coincident site lattice (CSL) grain boundaries with $\Sigma \leq 33$ in the FCC and BCC structures (cF and cI lattices). We use the same Σ cutoff as Morawiec because this range provides the best test of the hypothesis that large coincidence leads to low grain boundary energy. The maximum PCSD is 2.31 and the minimum is zero. The range $3 \leq \Sigma \leq 33$ includes the maximum PCSD as well as values less than one-tenth of the maximum (0.14), covering 94 % of the possible range. For comparison, we use the energies of Ni [9] and α-Fe [10] grain boundaries provided by continuous functions that provide the energies of any grain boundaries for which all five macroscopic parameters are supplied. These functions were fit to the energies of grain boundaries computed by molecular dynamics [11,12] and are consistent with experimental data [13]. For grain boundary relative area data, we will use data available in the grain boundary archive [14]. Throughout this letter, all boundaries are specified with the notation ω/[uvw]|(hkl), where ω is the misorientation angle, [uvw] is the axis of misorientation, and (hkl) is the grain boundary plane. This notation completely defines all five grain boundary parameters with no ambiguities.

Fig. 1 compares the PCSD for the first most dense and second most dense planes for all misorientations with $\Sigma \leq 33$ in the cF and cI lattices to the energy of grain boundaries in Ni and α-Fe. The data used in Figs. 1 and 2 are tabulated in Tables S1 through S4. Except for the fact that the twin boundaries in the cF (60.0°/[111]|(111)) and cI (60.0°/[111]|$(1\bar{2}1)$) lattices have the greatest PCSDs and the minimum energies, there is no apparent correlation between PCSD and grain boundary energy. When a line is fitted to the energies for the densest cF lattices, the "goodness of fit" $R^2 = 0.42$; this decreases to $R^2 = -0.03$ when the point

* Corresponding author.
E-mail address: gr20@andrew.cmu.edu (G.S. Rohrer).

https://doi.org/10.1016/j.mtla.2025.102453
Received 28 April 2025; Accepted 30 May 2025
Available online 1 June 2025

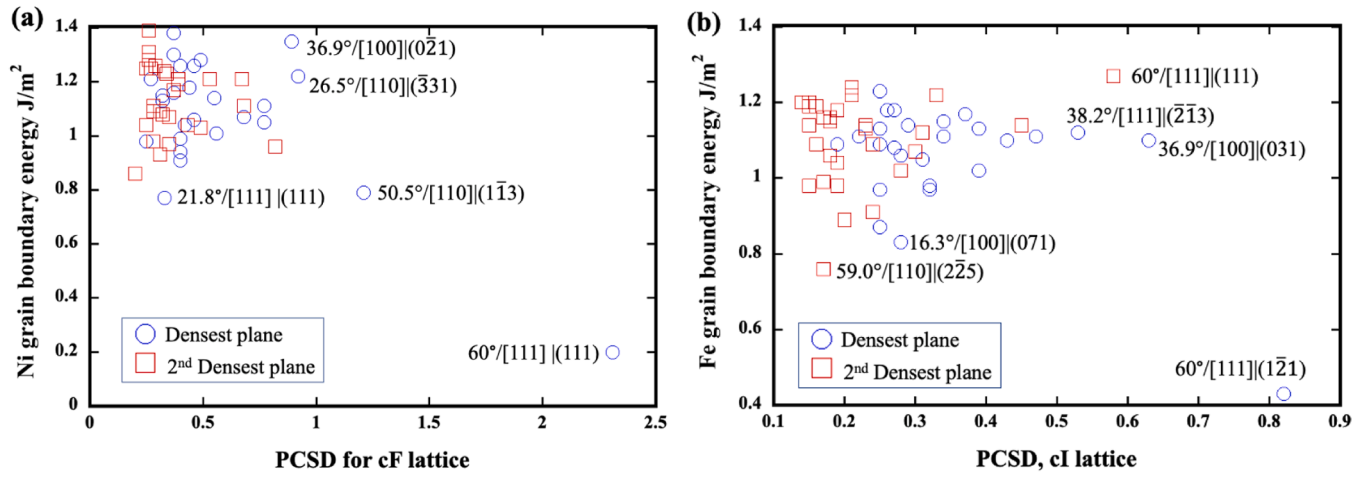

Fig. 1. Comparison of grain boundary energies to grain boundary PCSD for the two densest boundaries at each misorientation with $\Sigma \leq 33$. (a) Ni and (b) α-Fe. Each point represents the grain boundary energy and PCSD of a boundary with fixed misorientation and grain boundary plane orientation.

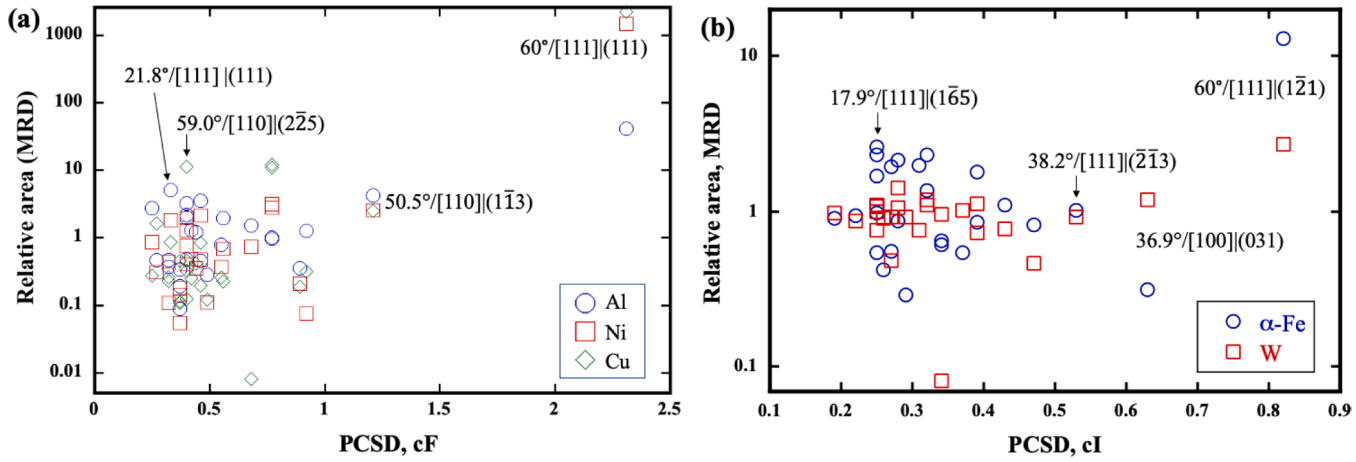

Fig. 2. PCSDs for the most dense planes for all misorientations with $\Sigma \leq 33$ in the cF and cI lattices are compared to the relative grain boundary area data. (a) Al, Ni, and Cu. (b) α-Fe and W.

for 60.0°/[111]|(111) is excluded. It is also noteworthy that the grain boundary with the second lowest energy (21.8°/[111]|(111)) has one of the lowest PCSDs and the grain boundaries with the third (26.5°/[110]|($\bar{3}$31)) and fourth (36.9°/[100]|(0$\bar{2}$1)) largest PCSDs have the largest grain boundary energies, contradicting the hypothesis that grain boundary energy and PCSD are inversely correlated. The energies of each grain boundary's second largest PCSD are also uncorrelated ($R^2 = -0.02$) to PCSD.

Analogous to the result for cF, there is no correlation between grain boundary energy and PCSD for boundaries between cI lattices. Fitting all of the densest points yields $R^2 = 0.23$ and if the twin is excluded it decreases to $R^2 = -0.03$. The second lowest energy grain boundary ((59.0/[110]|(2$\bar{2}$5))) has among the lowest PCSDs and the second (36.9°/[100]|(031)), third (60.0°/[111]|(111)), and fourth (38.2/[111]|($\bar{2}\bar{1}$3)) largest PCSDs have larger than average energies. Taken together, these results show no support for the hypothesis that the PCSD is a predictor of the grain boundary energy, consistent with Sutton and Balluffi's [3] conclusion.

The grain boundary energies in Fig. 1 were determined from functions [9,10] fit to discrete data [11,12]. This approach was taken because energies for many of the boundaries were not available in the original discrete data. A much richer set of grain boundary energies was recently computed for Al [5] that contains data for about 70 % of the boundaries considered here. When these energies are used in place of the interpolated energies, the agreement is not improved, as illustrated in Fig. S1. We note that grain boundary energies computed by simulation are sensitive to the assumed interatomic potential. However, it has been shown that while different potentials lead to different absolute values of the energy, the energy landscape (variation with crystallographic parameters) is almost unaffected by the potential [15]. Therefore, energy values computed by different potentials are expected to be proportional to those used here and not alter the conclusion.

A second way to seek a correlation between the PCSD and grain boundary energy is to examine the relative grain boundary areas. It has been found that in materials without significant texture that evolve by normal grain growth, the grain boundary relative area (λ) is inversely correlated with the grain boundary energy (γ), so that the observations approximate the following relation: $\lambda \propto \exp(-k\gamma)$, where k is a constant [16–18]. Therefore, if there is also an inverse correlation between PCSD and energy, we expect the relative area to obey the same relation, but with a positive sign in the exponent. To test this idea, existing relative grain boundary area data [16,19–22] available in the grain boundary data archive is examined [14].

Fig. 2 compares the PCSD for the most dense planes for all misorientations with $\Sigma \leq 33$ in the cF and cI lattices to the relative area data. The data in Fig. 2a compares the PCSDs for the cF lattice with three FCC metals, Al [22], Ni, and Cu [21]. Other than the fact that the coherent twin has the maximum relative area and PCSD, there is no other

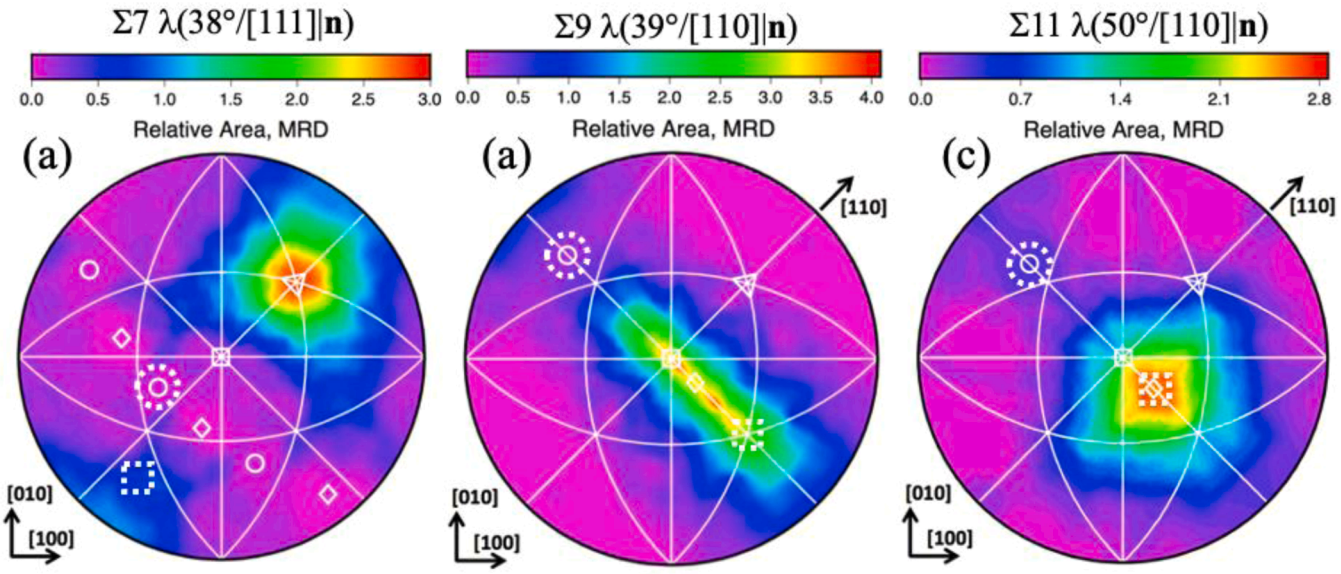

Fig. 3. Grain boundary plane distributions for the Σ7, Σ9, and Σ11 misorientations in Ni with the planes with the largest and second largest PCSD labeled. Each distribution is displayed in stereographic projection along the [001] axis, indicated by the white square in each plot. (a) For Σ7, the misorientation axis, [111], is marked by the triangle. The three white circles mark the orientations of the $(\bar{3}21)||(2\bar{3}1)$, $(\bar{2}13)||(3\bar{1}2)$, and $(1\bar{2}3)||(12\bar{3})$ boundaries and the three white diamonds mark the orientations of the $(\bar{5}14)||(5\bar{4}\bar{1})$, $(\bar{1}45)||(41\bar{5})$, and $(4\bar{5}1)||(\bar{1}5\bar{4})$ boundaries. The plane with the largest PCSD, $(\bar{3}5\bar{1})$, is marked with a dashed square and the plane with the second largest PCSD, $(\bar{2}\bar{1}3)$, is marked by a dashed circle. (b) For Σ9, the [110] misorientation axis is shown by the arrow. The white diamond (circle) marks the orientation of the $(1\bar{1}4)||(1\bar{1}\bar{4})$ $((\bar{2}21)||(2\bar{2}1))$ symmetric tilt grain boundary. The plane with the largest PCSD, $(1\bar{1}1)$, is marked with a dashed square and the plane with the second largest PCSD, $(\bar{2}21)$, is marked by a dashed circle. (c) For Σ11, the [110] misorientation axis is shown by the arrow. The white diamond (circle) marks the orientation of the $(1\bar{1}3)||(1\bar{1}\bar{3})$ $((\bar{3}32)||(3\bar{3}2))$ symmetric tilt grain boundary. The plane with the largest PCSD, $(1\bar{1}3)$, is marked with a dashed square and the plane with the second largest PCSD, $(\bar{3}32)$, is marked by a dashed circle.

apparent correlations in these data. For most of the data, the relative areas are spread over two orders of magnitude at a constant PCSD. The data in Fig. 2b compares the PCSDs for the cI lattice with two materials with this lattice, α-Fe [16] and W [20]. As for the cF lattice, there is no apparent correlation between the PCSD and the relative grain boundary area.

Finally, we compare the grain boundary planes with the largest and second largest PCSDs to selected grain boundary area distributions (see Fig. 3). For the Σ7 misorientation in Ni [21], we can see that both the largest and second largest PCSD planes do not coincide with the maximum and occur at relatively low points in the distribution. For the Σ9 misorientation, the largest PCSD is at a relatively large value, but not at the maximum. The second largest PCSD is at a minimum of area. For the Σ11 misorientation, the second largest PCSD is also at a minimum of area, but the largest PCSD is at the maximum. So, of the six possible boundaries, only one corresponds to a maximum in the distribution.

The present comparison of the PCSD to the grain boundary energy and population leads to the same conclusion reached by Sutton and Balluffi [3] – that the PCSD is not a predictor of grain boundary energy. In this case, the conclusion was confirmed from more extensive data and using a corrected formula to compute the PCSD. While this result will not be surprising to some, the presentation of these data is intended to convince those who still argue that PCSD is an indicator of low energy grain boundaries.

One might still argue that for especially large PCSDs, it might be an indicator of low energy. For example, the boundaries with the maximum PCSDs in the cF and cI lattices have the minimum energy (Fig. 1) and the usually have the maximum population (Fig. 2). However, support for such an argument is weak because there are only two boundaries in this subset of the data. Furthermore, that support is undermined by the fact that the minimum energy boundary in the cI lattice $(60.0°/[111]|(1\bar{2}1))$ has a PCSD of 0.82 while the $36.9°/[100]|(0\bar{2}1)$ boundary in the cF lattice has a PCSD of 0.89 and is one of the highest energy boundaries. In other words, a relatively large PCSD in the range of 0.89 does not automatically impart a low energy to a boundary.

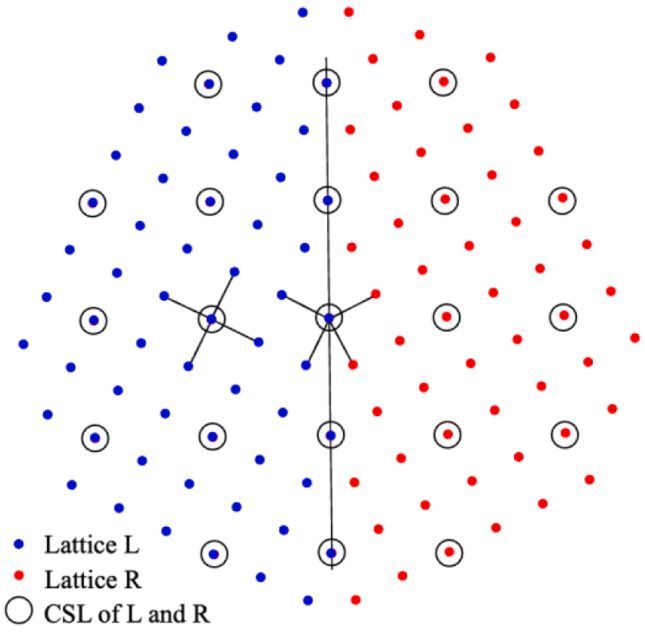

Fig. 4. Schematic depiction of the $36.9°/[100]|(0\bar{2}1)$ boundary in the cP lattice projected along the [001] direction. The coordination at the coincident sites at the boundary differs considerably from those in the bulk.

The $60.0°/[111]|(111)$ boundary might be considered an outlier in the sense that it has nearly twice the PCSD of the next highest boundary (2.31 for $60.0°/[111]|(111)$ and 1.21 for $50.5/[110]|(1\bar{1}3)$). This is probably the one boundary where planar coincidence has an impact on the energy. Because of the very special geometry of this boundary, the

first nearest neighbor coordination of the atoms in the boundary is unaltered. However, this is the only boundary where this is the case. As illustrated in Fig. 4 for the 36.9°/[100]|(0$\bar{2}$1) boundary, the coordination environment for the coincident sites at the boundary is nothing like it is in the bulk. In other words, the fact that atoms at the boundary are at coincident sites imparts no advantage with respect to a coordination environment that would lead to a reduced energy. From this perspective, it is not obvious why coincident sites should be connected to a low grain boundary energy, except for the special case of the 60.0°/[111]|(111) boundary in the cF lattice.

In summary, there is no evidence that the PCSD is related grain boundary energies or populations. This conclusion is based on boundaries with the largest and second largest PCSDs for CSL misorientations with $\Sigma \leq 33$ and reinforces the conclusion originally reached by Sutton and Balluffi [3].

CRediT authorship contribution statement

Eileen L. Hung: Writing – review & editing, Software, Investigation. **Zipeng Xu:** Software, Investigation. **Gregory S. Rohrer:** Writing – review & editing, Writing – original draft, Supervision, Project administration, Methodology, Funding acquisition, Conceptualization.

Declaration of competing interest

The author Gregory S. Rohrer is Coordinating Editor for Acta Materialia and was not involved in the editorial review or the decision to publish this article.

Acknowledgments

This work was supported by the National Science Foundation under DMREF Grant No 2118945.

Supplementary materials

Supplementary material associated with this article can be found, in the online version, at doi:10.1016/j.mtla.2025.102453.

References

[1] A.F. Acton, M. Bevis, Geometry of coincidence-site lattices, Acta Cryst. A A 27 (1971) 175–179, https://doi.org/10.1107/S0567739471000329.
[2] D.A. Smith, On the density of coincidence sites in grain boundaries, Scr. Metall. 8 (1974) 1197–1199, https://doi.org/10.1016/0036-9748(74)90494-3.
[3] A.P. Sutton, R.W. Balluffi, On geometric criteria for low interfacial energy, Acta Metall. 35 (1987) 2177–2201.
[4] A. Morawiec, On the determination of dense coincidence site lattice planes, Acta Cryst. A 78 (2022) 491–497, https://doi.org/10.1107/S2053273322008828.
[5] E.R. Homer, G.L.W. Hart, C. Braxton Owens, D.M. Hensley, J.C. Spendlove, L. H. Serafin, Examination of computed aluminum grain boundary structures and energies that span the 5D space of crystallographic character, Acta Mater. 234 (2022) 118006, https://doi.org/10.1016/j.actamat.2022.118006.
[6] A. Morawiec, Method to calculate the grain boundary energy distribution over the space of macroscopic boundary parameters from the geometry of triple junctions, Acta Mater. 48 (2000) 3525–3532.
[7] Y.F. Shen, X.T. Zhong, H. Liu, R.M. Suter, A. Morawiec, G.S. Rohrer, Determining grain boundary energies from triple junction geometries without discretizing the five-parameter space, Acta Mater. 166 (2019) 126–134, https://doi.org/10.1016/j.actamat.2018.12.022.
[8] G.S. Rohrer, Measuring and interpreting the structure of grain-boundary networks, J. Am. Ceram. Soc. 94 (2011) 633–646, https://doi.org/10.1111/j.1551-2916.2011.04384.x.
[9] V.V. Bulatov, B.W. Reed, M. Kumar, Grain boundary energy function for fcc metals, Acta Mater. 65 (2014) 161–175, https://doi.org/10.1016/j.actamat.2013.10.057.
[10] R. Sarochawikasit, C. Wang, P. Kumam, H. Beladi, T. Okita, G.S. Rohrer, S. Ratanaphan, Grain boundary energy function for alpha iron, Materialia 19 (2021), https://doi.org/10.1016/j.mtla.2021.101186.
[11] D.L. Olmsted, S.M. Foiles, E.A. Holm, Survey of computed grain boundary properties in face-centered cubic metals: I. Grain boundary energy, Acta Mater. 57 (2009) 3694–3703, https://doi.org/10.1016/j.actamat.2009.04.007.
[12] S. Ratanaphan, D.L. Olmsted, V.V. Bulatov, E.A. Holm, A.D. Rollett, G.S. Rohrer, Grain boundary energies in body-centered cubic metals, Acta Mater. 88 (2015) 346–354, https://doi.org/10.1016/j.actamat.2015.01.069.
[13] G.S. Rohrer, E.A. Holm, A.D. Rollett, S.M. Foiles, J. Li, D.L. Olmsted, Comparing calculated and measured grain boundary energies in nickel, Acta Mater. 58 (2010) 5063–5069, https://doi.org/10.1016/j.actamat.2010.05.042.
[14] G.S. Rohrer, Grain Boundary Data Archive. http://mimp.materials.cmu.edu/~gr20/Grain_Boundary_Data_Archive/, 2015.
[15] B. Waters, D.S. Karls, I. Nikiforov, R.S. Elliott, E.B. Tadmor, B. Runnels, Automated determination of grain boundary energy and potential-dependence using the OpenKIM framework, Comp. Mater. Sci. 220 (2023), https://doi.org/10.1016/j.commatsci.2023.112057.
[16] H. Beladi, G.S. Rohrer, The relative grain boundary area and energy distributions in a ferritic steel determined from three-dimensional electron backscatter diffraction maps, Acta Mater. 61 (2013) 1404–1412, https://doi.org/10.1016/j.actamat.2012.11.017.
[17] J. Li, S.J. Dillon, G.S. Rohrer, Relative grain boundary area and energy distributions in nickel, Acta Mater. 57 (2009) 4304–4311, https://doi.org/10.1016/j.actamat.2009.06.004.
[18] D.M. Saylor, A. Morawiec, G.S. Rohrer, The relative free energies of grain boundaries in magnesia as a function of five macroscopic parameters, Acta Mater. 51 (2003) 3675–3686, https://doi.org/10.1016/S1359-6454(03)00182-4.
[19] S.J. Dillon, G.S. Rohrer, Characterization of the grain-boundary character and energy distributions of Yttria using automated serial sectioning and EBSD in the FIB, J. Am. Ceram. Soc. 92 (2009) 1580–1585, https://doi.org/10.1111/j.1551-2916.2009.03064.x.
[20] X. Liu, D. Choi, H. Beladi, N.T. Nuhfer, G.S. Rohrer, K. Barmak, The five-parameter grain boundary character distribution of nanocrystalline tungsten, Scripta Mater 69 (2013) 413–416, https://doi.org/10.1016/j.scriptamat.2013.05.046.
[21] V. Randle, G.S. Rohrer, H.M. Miller, M. Coleman, G.T. Owen, Five-parameter grain boundary distribution of commercially grain boundary engineered nickel and copper, Acta Mater. 56 (2008) 2363–2373, https://doi.org/10.1016/j.actamat.2008.01.039.
[22] D.M. Saylor, B.S. El Dasher, A.D. Rollett, G.S. Rohrer, Distribution of grain boundaries in aluminum as a function of five macroscopic parameters, Acta Mater. 52 (2004) 3649–3655, https://doi.org/10.1016/j.actamat.2004.04.018.

Supplemental information for:
Planar Coincident Site Density is Not a Reliable Predictor of Grain Boundary Energy

Eileen L. Hung, Zipeng Xu, and Gregory S. Rohrer

Department of Materials Science and Engineering, Carnegie Mellon University, Pittsburgh, PA 15213

Table S1 contains the data used to plot Figure 1(a) and Figure S1. The densest and second densest planes are from reference [1] and the aluminum grain boundaries energies are from reference [2]. The nickel grain boundary energies are computed using the results of reference [3]. The planar coincident site density for the cF lattice is calculated following reference [1]. Specifically:

$$\mathrm{PCSD} = \frac{4}{\sqrt{\beta_{hkl}\Sigma}}$$

Where β_{hkl} and Σ (inverse lattice coincidence) are factors defined in reference [1] and listed in Table S1.

Table S2 contains the data used to plot Figure 1(b). The densest and second densest planes are from reference [1] and the α-Fe grain boundary energies are computed using the results of reference [4]. The planar coincident site density for the cI lattice is calculated following reference [1]. Specifically:

$$\mathrm{PCSD} = \frac{2}{\sqrt{\beta_{hkl}\Sigma}}$$

Where β_{hkl} and Σ (inverse lattice coincidence) are listed in Table S2.

Table S1. PCSD and grain boundary energy data for the cF lattice

Σ	First densest	β_{hkl}	PCSD	γ_{Ni} J/m^2	γ_{Al} J/m^2	Second densest	β_{hkl}	PCSD	γ_{Ni} J/m^2	γ_{Al} J/m^2
3	$(111)\|\|(\bar{1}\bar{1}\bar{1})$	1	2.31	0.20	0.08	$(1\bar{2}1)\|\|(11\bar{2})$	8	0.82	0.96	0.35
5	$(0\bar{2}1)\|\|(01\bar{2})$	4	0.89	1.35	0.94	$(531)\|\|(\bar{5}\bar{3}1)$	7	0.68	1.11	
7	$(\bar{3}\bar{5}1)\|\|(53\bar{1})$	5	0.68	1.07	0.35	$(\bar{2}\bar{1}3)\|\|(3\bar{1}\bar{2})$	8	0.53	1.21	0.46
9	$(1\bar{1}1)\|\|(\bar{1}1\bar{5})$	3	0.77	1.11		$(\bar{2}21)\|\|(2\bar{2}1)$	4	0.67	1.21	0.45
11	$(1\bar{1}3)\|\|(1\bar{1}\bar{3})$	1	1.2	0.79	0.15	$(\bar{3}32)\|\|(3\bar{3}2)$	8	0.43	1.04	0.39
13a	$(023)\|\|(0\bar{3}\bar{2})$	4	0.55	1.14	0.43	$(051)\|\|(0\bar{5}1)$	8	0.39	1.21	0.49
13b	$(931)\|\|(\bar{9}\bar{1}\bar{3})$	7	0.42	1.04	0.52	$(\bar{4}31)\|\|(3\bar{4}1)$	8	0.39	1.19	0.47
15	$(\bar{1}\bar{1}1)\|\|(71\bar{5})$	5	0.46	1.26		$(1\bar{2}5)\|\|(1\bar{2}\bar{5})$	8	0.37	1.17	0.43
17a	$(041)\|\|(0\bar{4}1)$	4	0.49	1.28	0.49	$(0\bar{5}3)\|\|(03\bar{5})$	8	0.34	1.23	0.47
17b	$(155)\|\|(\bar{1}\bar{7}\bar{1})$	3	0.56	1.01	0.32	$(\bar{3}22)\|\|(2\bar{3}2)$	4	0.49	1.03	0.37
19a	$(\bar{3}31)\|\|(3\bar{3}1)$	1	0.92	1.22	0.43	$(1\bar{1}6)\|\|(1\bar{1}\bar{6})$	8	0.32	1.08	0.39
19b	$(\bar{5}32)\|\|(3\bar{5}2)$	8	0.32	1.13	0.47	$(11\ 17)\|\|(\bar{7}\bar{1}\ \bar{1}1)$	9	0.31	0.93	
21a	$(111)\|\|(\bar{1}\bar{1}\bar{1})$	7	0.3	0.77	0.21	$(\bar{4}\bar{1}5)\|\|(5\bar{1}\bar{4})$	8	0.31	1.09	0.45
21b	$(1\bar{4}2)\|\|(12\bar{4})$	4	0.4	1.18	0.44	$(\bar{1}11)\|\|(5\ \bar{1}\bar{1}\ 1)$	7	0.33	1.24	
23	$(359)\|\|(\bar{3}\bar{9}\bar{5})$	5	0.37	1.30		$(1\bar{6}3)\|\|(13\bar{6})$	8	0.29	1.26	
25a	$(0\bar{4}3)\|\|(03\bar{4})$	4	0.40	0.94	0.39	$(071)\|\|(0\bar{7}1)$	8	0.28	0.98	0.471
25b	$(517)\|\|(\bar{1}\bar{5}\bar{7})$	3	0.46	1.06	0.50	$(\bar{4}53)\|\|(4\bar{5}3)$	8	0.28	1.09	
27a	$(1\bar{1}5)\|\|(1\bar{1}\bar{5})$	1	0.77	1.05	0.36	$(\bar{5}52)\|\|(5\bar{5}2)$	8	0.27	1.25	
27b	$(1\bar{2}7)\|\|(1\bar{2}\bar{7})$	8	0.27	1.21	0.52	$(\bar{5}11)\|\|(5\bar{1}1)$	9	0.26	1.31	0.53
						$(111)\|\|(\bar{7}\ \bar{1}\bar{3}\ \bar{5})$	9	0.26	1.28	
29a	$(052)\|\|(0\bar{5}\bar{2})$	4	0.37	1.38	0.51	$(037)\|\|(0\bar{7}\bar{3})$	8	0.26	1.39	0.52
29b	$(\bar{4}32)\|\|(3\bar{4}2)$	4	0.37	1.16		$(11\ \bar{1}9)\|\|(\bar{5}\bar{3}\ \bar{1}\bar{3})$	7	0.28	1.11	
31a	$(1\bar{6}5)\|\|(15\bar{6})$	8	0.25	0.98		$(13\ 15\ 3)\|\|(\bar{1}\bar{5}\ \bar{1}\bar{3}\ \bar{3})$	13	0.20	0.86	
31b	$(\bar{7}95)\|\|(3\ \bar{1}\bar{1}\ 5)$	5	0.32	1.15		$(2\bar{7}3)\|\|(23\bar{7})$	8	0.25	1.04	
33a	$(5\bar{5}7)\|\|(\bar{1}1\bar{3})$	3	0.40	0.99		$(\bar{4}41)\|\|(4\bar{4}1)$	4	0.35	1.07	0.42
33b	$(311)\|\|(\bar{3}\bar{1}\bar{1})$	3	0.40	1.26	0.47	$(1\bar{7}4)\|\|(14\bar{7})$	8	0.25	1.25	0.54
33c	$(7\bar{7}1)\|\|(\bar{1}1\bar{3})$	3	0.40	0.91	0.30	$(2\bar{2}5)\|\|(2\bar{2}\bar{5})$	4	0.35	0.97	0.32

Table S2. PCSD and grain boundary energy data for the cI lattice

Σ	First densest	β_{hkl}	PCSD	γ_{Fe}	Second densest	β_{hkl}	PCSD	γ_{Fe}
3	$(1\bar{2}1)\|\|(11\bar{2})$	2	0.82	0.43	$(111)\|\|(\bar{1}\bar{1}\bar{1})$	4	0.58	1.27
5	$(031)\|\|(0\bar{3}1)$	2	0.63	1.10	$(0\bar{2}1)\|\|(01\bar{2})$	4	0.45	1.14
7	$(\bar{2}\bar{1}3)\|\|(3\bar{1}\bar{2})$	2	0.53	1.12	$(\bar{1}\bar{4}5)\|\|(4\bar{1}\bar{5})$	6	0.31	1.12
9	$(1\bar{1}4)\|\|(1\bar{1}\bar{4})$	2	0.47	1.11	$(\bar{2}21)\|\|(2\bar{2}1)$	4	0.33	1.22
11	$(\bar{3}32)\|\|(3\bar{3}2)$	2	0.43	1.10	$(1\bar{1}3)\|\|(1\bar{1}\bar{3})$	4	0.30	1.07
13a	$(051)\|\|(0\bar{5}1)$	2	0.39	1.02	$(023)\|\|(0\bar{3}\bar{2})$	4	0.28	1.02
13b	$(\bar{4}31)\|\|(3\bar{4}1)$	2	0.39	1.13	$(\bar{7}25)\|\|(7\bar{5}\bar{2})$	6	0.23	1.14
15	$(1\bar{2}5)\|\|(1\bar{2}\bar{5})$	2	0.37	1.17	$(\bar{3}10)\|\|(8\bar{1}5)$	6	0.21	1.24
					$(130)\|\|(\bar{4}\bar{7}5)$	6	0.21	1.22
17a	$(0\bar{5}3)\|\|(03\bar{5})$	2	0.34	1.11	$(041)\|\|(0\bar{4}1)$	4	0.24	1.09
17b	$(433)\|\|(\bar{3}\bar{4}\bar{3})$	2	0.34	1.15	$(\bar{3}22)\|\|(2\bar{3}2)$	4	0.24	0.91
19a	$(1\bar{1}6)\|\|(1\bar{1}\bar{6})$	2	0.32	0.98	$(\bar{3}31)\|\|(3\bar{3}1)$	4	0.23	1.13
19b	$(\bar{5}32)\|\|(3\bar{5}2)$	2	0.32	0.97	$(\bar{1}\bar{7}8)\|\|(71\bar{8})$	6	0.19	0.98
21a	$(\bar{4}\bar{1}5)\|\|(5\bar{1}\bar{4})$	2	0.31	1.05	$(\bar{1}\bar{2}3)\|\|(21\bar{3})$	6	0.18	1.06
21b	$(1\bar{4}2)\|\|(12\bar{4})$	4	0.22	1.11	$(\bar{3}\bar{2}1)\|\|(11\ 1\bar{2})$	6	0.18	1.15
					$(123)\|\|(\bar{5}\ \bar{1}0\ \bar{1})$	6	0.18	1.16
					$(\bar{2}13)\|\|(2\bar{3}\bar{1})$	6	0.18	1.15
23	$(1\bar{6}3)\|\|(13\bar{6})$	2	0.29	1.14	$(\bar{5}78)\|\|(4\ \bar{1}1\ \bar{1})$	6	0.17	1.16
25a	$(071)\|\|(0\bar{7}1)$	2	0.28	0.83	$(0\bar{4}3)\|\|(03\bar{4})$	4	0.20	0.89
25b	$(\bar{4}53)\|\|(4\bar{5}3)$	2	0.28	1.06	$(\bar{1}0\ \bar{7}1)\|\|(11\ 52)$	6	0.16	1.09
27a	$(\bar{5}52)\|\|(5\bar{5}2)$	2	0.27	1.18	$(1\bar{1}5)\|\|(1\bar{1}\bar{5})$	4	0.19	1.04
27b	$(1\bar{2}7)\|\|(1\bar{2}\bar{7})$	2	0.27	1.08	$(411)\|\|(5\bar{1}1)$	6	0.16	1.19
29a	$(037)\|\|(0\bar{7}\bar{3})$	2	0.26	1.18	$(052)\|\|(0\bar{5}\bar{2})$	4	0.19	1.18
29b	$(\bar{4}32)\|\|(3\bar{4}2)$	4	0.19	1.09	$(72\ 11)\|\|(\bar{2}\bar{7}\ \bar{1}\bar{1})$	6	0.15	1.19
					$(\bar{1}0\ \bar{7}5)\|\|(13\ 2\bar{1})$	6	0.15	1.14
31a	$(1\bar{6}5)\|\|(15\bar{6})$	2	0.25	0.97	$(\bar{4}\bar{7}\ 11)\|\|(74\ \bar{1}\bar{1})$	6	0.15	0.98
31b	$(2\bar{7}3)\|\|(23\bar{7})$	2	0.25	1.09	$(13\ 14)\|\|(\bar{1}\bar{1}\ \bar{1}\bar{8})$	6	0.15	1.20
33a	$(1\bar{1}8)\|\|(1\bar{1}\bar{8})$	2	0.25	0.87	$(\bar{4}41)\|\|(4\bar{4}1)$	4	0.17	0.99
33b	$(1\bar{7}4)\|\|(14\bar{7})$	2	0.25	1.13	$(\bar{2}33)\|\|(5\ \bar{1}3\ \bar{2})$	6	0.14	1.20
33c	$(\bar{5}54)\|\|(5\bar{5}4)$	2	0.25	1.23	$(2\bar{2}5)\|\|(2\bar{2}\bar{5})$	4	0.17	0.76

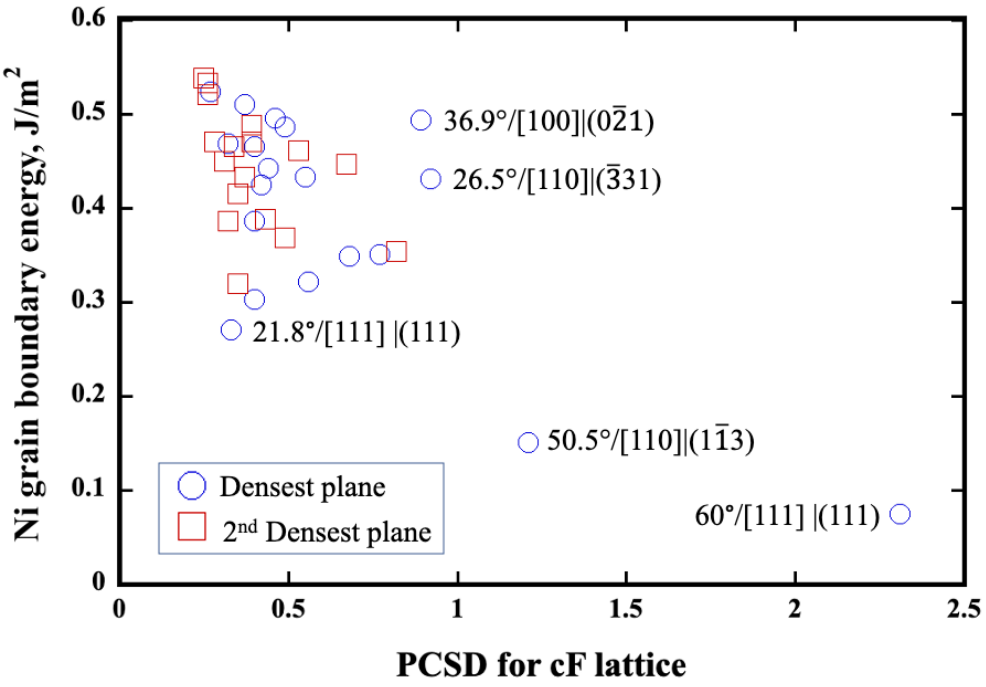

Figure S1. Comparison of Al grain boundary energies to grain boundary PCSD for the two densest boundaries at each misorientation with $\Sigma \leq 33$.

Table S3. PCSD and relative area data for the cF lattice

Σ	First densest	β_{hkl}	PCSD	Al Area, MRD	Ni Area, MRD	Cu Area, MRD
3	$(111)\|\|(\bar{1}\bar{1}\bar{1})$	1	2.31	41.4	1490	2240
5	$(0\bar{2}1)\|\|(01\bar{2})$	4	0.89	0.353	0.211	0.186
7	$(\bar{3}\bar{5}1)\|\|(53\bar{1})$	5	0.68	1.51	0.742	0.0080
9	$(1\bar{1}1)\|\|(\bar{1}1\bar{5})$	3	0.77	1.01	2.81	11.1
11	$(1\bar{1}3)\|\|(1\bar{1}\bar{3})$	1	1.2	4.28	2.56	2.52
13a	$(023)\|\|(0\bar{3}\bar{2})$	4	0.55	0.787	0.370	0.259
13b	$(931)\|\|(\bar{9}1\bar{3})$	7	0.42	1.30	0.491	0.253
15	$(\bar{1}\bar{1}1)\|\|(71\bar{5})$	5	0.46	0.454	0.474	0.194
17a	$(041)\|\|(0\bar{4}1)$	4	0.49	0.280	0.111	0.121
17b	$(155)\|\|(\bar{1}\bar{7}\bar{1})$	3	0.56	1.96	0.683	0.222
19a	$(\bar{3}31)\|\|(3\bar{3}1)$	1	0.92	1.26	0.0760	0.313
19b	$(\bar{5}32)\|\|(3\bar{5}2)$	8	0.32	0.368	0.109	0.256
21a	$(111)\|\|(\bar{1}\bar{1}\bar{1})$	7	0.3	5.10	1.84	0.861
21b	$(1\bar{4}2)\|\|(12\bar{4})$	4	0.4	1.20	0.356	0.417
23	$(359)\|\|(\bar{3}\bar{9}\bar{5})$	5	0.37	0.341	0.0550	0.459
25a	$(0\bar{4}3)\|\|(03\bar{4})$	4	0.40	1.9800	0.777	0.459
25b	$(517)\|\|(\bar{1}\bar{5}\bar{7})$	3	0.46	3.5580	2.14	0.837
27a	$(1\bar{1}5)\|\|(1\bar{1}\bar{5})$	1	0.77	0.955	3.13	12.1
27b	$(1\bar{2}7)\|\|(1\bar{2}\bar{7})$	8	0.27	0.460	0.310	1.62
29a	$(052)\|\|(0\bar{5}\bar{2})$	4	0.37	0.191	0.179	0.107
29b	$(\bar{4}32)\|\|(3\bar{4}2)$	4	0.37	0.0890	0.143	0.114
31a	$(1\bar{6}5)\|\|(15\bar{6})$	8	0.25	2.72	0.866	0.276
31b	$(\bar{7}95)\|\|(3\ \bar{1}\bar{1}\ 5)$	5	0.32	0.465	0.446	0.231
33a	$(5\bar{5}7)\|\|(\bar{1}1\bar{3})$	3	0.40	2.21	1.29	0.320
33b	$(311)\|\|(\bar{3}\bar{1}\bar{1})$	3	0.40	0.478	0.409	0.123
33c	$(7\bar{7}1)\|\|(\bar{1}1\bar{3})$	3	0.40	3.21	1.97	11.3

Table S4. PCSD and relative area data for the cI lattice

Σ	First densest	β_{hkl}	PCSD	Fe Area, MRD	W Area, MRD
3	$(1\bar{2}1)\|\|(11\bar{2})$	2	0.82	13.1	2.71
5	$(031)\|\|(0\bar{3}1)$	2	0.63	0.313	1.18
7	$(\bar{2}\bar{1}3)\|\|(3\bar{1}\bar{2})$	2	0.53	1.00	0.912
9	$(1\bar{1}4)\|\|(1\bar{1}\bar{4})$	2	0.47	0.808	0.458
11	$(\bar{3}32)\|\|(3\bar{3}2)$	2	0.43	1.10	0.763
13a	$(051)\|\|(0\bar{5}1)$	2	0.39	0.840	1.11
13b	$(\bar{4}31)\|\|(3\bar{4}1)$	2	0.39	1.78	0.723
15	$(1\bar{2}5)\|\|(1\bar{2}\bar{5})$	2	0.37	0.544	1.02
17a	$(0\bar{5}3)\|\|(03\bar{5})$	2	0.34	0.608	0.953
17b	$(433)\|\|(\bar{3}\bar{4}\bar{3})$	2	0.34	0.644	0.0800
19a	$(1\bar{1}6)\|\|(1\bar{1}\bar{6})$	2	0.32	2.30	1.08
19b	$(\bar{5}32)\|\|(3\bar{5}2)$	2	0.32	1.36	1.19
21a	$(\bar{4}\bar{1}5)\|\|(5\bar{1}\bar{4})$	2	0.31	1.96	0.758
21b	$(1\bar{4}2)\|\|(12\bar{4})$	4	0.22	0.937	0.860
23	$(1\bar{6}3)\|\|(13\bar{6})$	2	0.29	0.287	0.913
25a	$(071)\|\|(0\bar{7}1)$	2	0.28	2.15	1.04
25b	$(\bar{4}53)\|\|(4\bar{5}3)$	2	0.28	0.872	1.40
27a	$(\bar{5}52)\|\|(5\bar{5}2)$	2	0.27	1.94	0.475
27b	$(1\bar{2}7)\|\|(1\bar{2}\bar{7})$	2	0.27	0.552	0.914
29a	$(037)\|\|(0\bar{7}\bar{3})$	2	0.26	0.415	0.894
29b	$(\bar{4}32)\|\|(3\bar{4}2)$	4	0.19	0.895	0.969
31a	$(1\bar{6}5)\|\|(15\bar{6})$	2	0.25	2.58	1.09
31b	$(2\bar{7}3)\|\|(23\bar{7})$	2	0.25	0.973	1.07
33a	$(1\bar{1}8)\|\|(1\bar{1}\bar{8})$	2	0.25	2.30	1.08
33b	$(1\bar{7}4)\|\|(14\bar{7})$	2	0.25	0.542	0.757
33c	$(\bar{5}54)\|\|(5\bar{5}4)$	2	0.25	1.67	0.994

References Cited

[1] A. Morawiec. On the determination of dense coincidence site lattice planes, Acta Cryst A 78 (2022) 491-497, http://dx.doi.org/10.1107/S2053273322008828.

[2] E.R. Homer, G.L.W. Hart, C. Braxton Owens, D.M. Hensley, J.C. Spendlove, L.H. Serafin. Examination of computed aluminum grain boundary structures and energies that span the 5D space of crystallographic character, Acta Mater 234 (2022) 118006, http://dx.doi.org/https://doi.org/10.1016/j.actamat.2022.118006.

[3] V.V. Bulatov, B.W. Reed, M. Kumar. Grain boundary energy function for fcc metals, Acta Mater. 65 (2014) 161-175, http://dx.doi.org/10.1016/j.actamat.2013.10.057.

[4] R. Sarochawikasit, C. Wang, P. Kumam, H. Beladi, T. Okita, G.S. Rohrer, S. Ratanaphan. Grain boundary energy function for alpha iron, Materialia 19 (2021), http://dx.doi.org/10.1016/j.mtla.2021.101186.